

Low-energy properties of two-dimensional magnetic nanostructures: interparticle interactions and disorder effects

P J Jensen[‡] and G M Pastor

Laboratoire de Physique Quantique, Université Paul Sabatier,
Centre National de la Recherche Scientifique,
118, route de Narbonne, F-31062 Toulouse, France

E-mail: jensen@physik.fu-berlin.de
gustavo.pastor@irsamc.ups-tlse.fr

16 November 2018

Abstract. The low-energy properties of two-dimensional ensembles of dipole-coupled magnetic nanoparticles are studied as function of structural disorder and particle coverage. Already small deviations from a square particle arrangement lift the degeneracies of the microvortex magnetic configuration, and result in a strongly noncollinear magnetic order of the particle ensemble. The energy distribution of metastable states is determined. For a low degree of disorder a strongly asymmetric shape with a pronounced peak of the ground state energy results. In contrast, for a strong disorder a Gaussian-like distribution is obtained. The average dipole coupling energy $\overline{E}_{\text{dip}}$ decreases with increasing structural disorder. The role of vacancies has been studied for a square particle array by determining the angular distribution of the preferred microvortex angle as function of the vacancy concentration. Indications for a preferred angular direction along the axial as well as along the diagonal directions of the square array are revealed. A corresponding investigation for disturbed square arrays results in a different angular distribution. The effect of dipole-quadrupole corrections resulting from the finite size of the particles is quantified.

PACS numbers: 75.75.+a, 75.70.Ak, 75.50.Lk, 61.46.+w

Submitted to: *New J. Phys.*

[‡] Corresponding author. On leave from: Institut für Theoretische Physik, Freie Universität Berlin, Arnimallee 14, D-14195 Berlin, Germany.

1. Introduction

Interacting magnetic nanostructured materials are currently the subject of intense research activity, driven by their fundamental interest and technological perspectives [1]. Numerous experimental and theoretical studies have been performed for various two-dimensional (2D) [2] and three-dimensional (3D) [3, 4, 5, 6, 7, 8] arrangements of nanometer-size magnetic particles having different degrees of structural and magnetic disorder. The magnetic behaviour of these systems is determined by single-particle properties (e.g., particle moments, lattice and shape anisotropies, etc.), by the composition and morphology of the nanostructure, and in particular by the nature of the dominant interparticle interactions. The latter comprises especially the magnetic dipole coupling, which will be addressed in the present study. Other interparticle interactions are, for example, the Rudermann-Kittel-Kasuya-Yosida (RKKY) indirect exchange mediated by the conduction electrons of a metallic substrate, or the short-range direct exchange in case when the particles are in contact. The relative importance of single-particle versus interparticle contributions can be tuned experimentally at least to some extent by changing sample characteristics such as the particle-size distribution or the average interparticle distance. For low particle coverages the interactions can be treated as a perturbation to the single-particle properties. However, for dense particle ensembles the interparticle interactions become increasingly important and eventually dominate. In this interesting case the single-particle approach is no longer applicable and an explicit treatment of the interactions is unavoidable [3, 4, 5].

A fundamental question in this context is to identify and understand the collectively ordered magnetic states which are induced by the interactions in such particle ensembles. A few basic properties of strictly periodic dipole-coupled systems are summarized. The ground state of a *square* lattice of equal-sized (monodispersed) particles is the so-called *microvortex* (MV) magnetic arrangement [9, 10]. This magnetic structure is characterized by the microvortex angle ϕ_{mv} , where the angles of the particle magnetizations of a plaquette of four neighbouring particles are given by $\phi_1 = \phi_{mv}$, $\phi_2 = -\phi_{mv}$, $\phi_3 = 180^\circ + \phi_{mv}$, and $\phi_4 = 180^\circ - \phi_{mv}$. In particular, multiples of $\phi_{mv} = 90^\circ$ represent *columnar* states, consisting of ferromagnetic rows or columns with alternating signs of magnetizations. Evidently, the MV state has a vanishing net magnetization. The parallel or ferromagnetic (FM) state has a larger energy and is actually an unstable solution. The ordering of dipole-coupled spins is very sensitive to the lattice structure. For example, the honeycomb lattice has a ground state with a vanishing net magnetization which is similar to the MV state of the square lattice [10]. In contrast, for the hexagonal lattice the ground state is ferromagnetic [11, 12].

Despite the fact that the dipole interaction is not rotationally invariant, the ground state of these dipole-coupled periodic particle arrays are continuously degenerate with respect to a rotation of the MV angle ϕ_{mv} or of the FM angle ϕ_{fm} , respectively. This holds for classical spins at $T = 0$. Thermal fluctuations, quantum fluctuations, or a structural disorder immediately lift these accidental ground state degeneracies of the periodic structures. The energy lowering associated to the symmetry breaking stabilizes the system in some particular magnetic order. Therefore, the

square and honeycomb lattices are said to show a so-called 'order-by-disorder' effect [10, 13]. This implies that internal (nontrivial) degeneracies (e.g., the relative directions of magnetic sublattices) are lifted by the presence of disorder, and that particular directions of the sublattice magnetizations are preferred. Moreover, for a dipole-coupled square lattice the fluctuations induce a fourfold in-plane magnetic anisotropy. As shown by Prakash and Henley [10], the preferred in-plane magnetic orientations are the axial directions (columnar states) for thermal and quantum fluctuations, and the diagonal directions for a structural disorder induced by a small amount of vacancies. In addition, Monte Carlo calculations and interacting spin wave theory indicate that a magnetic ordering at finite temperatures exists for a dipole-coupled square spin lattice, since the magnetic excitations are not continuously degenerate [14]. Thus, the Mermin-Wagner theorem, which excludes an ordered state for a continuously degenerate 2D system at finite temperatures [15], is not effective in this case. Notice that already the *long-range* character of the dipole interaction induces a collectively ordered magnetic state in a square lattice [16].

Structural disorder, which is usually present in real magnetic nanostructures, results for example from the size and shape dispersion, positional disorder, or random anisotropy axes. Due to the nonuniform and competing nature of the magnetic couplings the magnetic ordering in disordered particle ensembles is similar to the one of a spin-glass [17]. Thus, many different metastable states exist, which are characterized by strong magnetic noncollinearities. An intriguing question in this context is whether the dipole interaction in *disordered* planar particle ensembles results in a collectively ordered magnetic state. Several experiments on interacting, high-density ferrofluid systems indicate the onset of a collectively ordered state below a characteristic, concentration-dependent temperature. For example, at this temperature a 'critical slowing down' of the magnetic relaxation is observed [3, 4]. Furthermore, recent measurements on Co islands on Cu(001) exhibit a magnetic hysteresis and remanence in the temperature range up to 150 K also for coverages below the magnetic percolation threshold [18]. Due to the small size of the Co islands these findings could not be explained simply by single-particle blocking effects. Note that the experimental determination of the ordering temperature is difficult, since the relaxation times are often very long. Hence, it is of considerable interest to analyze how the magnetic order depends on the sample parameters which can be controlled in experiment.

The purpose of this paper is the theoretical study of the low-energy properties of dipole-coupled magnetic particle ensembles forming inhomogeneous planar arrangements with various degrees of disorder ranging from a quasi-periodic square lattice to a random array. Numerical simulations are performed in order to achieve a detailed microscopic description within the model. The low symmetry of the system and the complicated nature of the interaction seem to preclude simple analytical approaches. We focus on the strongly interacting case, neglecting single-particle anisotropies. Special attention is paid to the role of disorder and noncollinear arrangements of the particle magnetic moments. In particular, we determine the energy distribution of metastable states and the average magnetic dipole energy for different coverages and types of disorder. Furthermore, we investigate global and local order parameters as function of disorder, and compare our results with previous

calculations [10]. All calculations are performed at $T = 0$.

The rest of the paper is organized as follows. The theoretical methods are outlined in section 2. Representative results for the magnetic arrangements, as well as for various magnetic properties are presented in section 3. A conclusion is given in section 4. Finally, in the Appendix we report details for the extension of the dipole summation beyond the point-dipole approximation which takes into account effects resulting from the finite particle size.

2. Theory

We consider a 2D rectangular unit cell in the xy - plane with $n = n_x \times n_y$ non-overlapping, disk-shaped magnetic particles. Due to the strong direct exchange interaction and the small size of the particles under consideration, each particle i can be viewed as a single magnetic domain (Stoner-Wohlfarth particle) [19]. Thus, a particle containing N_i atoms carries a giant spin $M_i = N_i \mu_{at}$, where μ_{at} is the atomic magnetic moment. For simplicity, we restrict the particle magnetizations to be confined to the xy plane, the planar rotator \mathbf{M}_i is then characterized by the in-plane angle ϕ_i : $\mathbf{M}_i = (M_i^x, M_i^y, M_i^z) = M_i(\cos \phi_i, \sin \phi_i, 0)$. In this study no size dispersion is considered, i.e., $N_i = N$. For disk-shaped particles the particle radius r_0 is given by $r_0/a_0 = \sqrt{N}$, where a_0 is the interatomic distance. Unless otherwise stated, the present results refer to a unit cell containing $n = 100$ particles with $N = 1000$ atoms each. The size of the unit cell is given by $L_x \times L_y = (n_x R_0) \times (n_y R_0)$, with R_0 the average interparticle distance. For a planar array of circular particles the overall surface coverage is $C = \pi(r_0/R_0)^2$. Four different types of the lateral particle arrangement have been considered: (i) a periodic square array, i.e., the particle centers are located on the sites of a square lattice with lattice constant R_0 , (ii) a disturbed (quasi-periodic) array for which the particle centers deviate randomly from the square array, using a Gaussian distribution $P(\mathbf{R})$ with positional standard deviation σ_R , (iii) a diluted square particle lattice containing a number of vacancies n_{vac} with concentration C_{vac} , and (iv) a fully random distribution of non-overlapping particles within the unit cell. Periodic boundary conditions are introduced in order to describe an infinitely extended planar particle ensemble. By considering a single unit cell a finite system can be realized as well. In this case the effect of boundaries will strongly dominate the resulting magnetic arrangement.

For such particle ensembles we consider the dipole-dipole interaction between the magnetic moments \mathbf{M}_i , which can also be expressed in terms of a dipole field $\mathbf{B}_i^{\text{dip}}$ acting on \mathbf{M}_i due to all other particle magnetic moments:

$$E_{\text{dip}} = \frac{\mu_0}{2} \sum_{\substack{i,j \\ i \neq j}} [\mathbf{M}_i \cdot \mathbf{M}_j r_{ij}^{-3} - 3(\mathbf{r}_{ij} \cdot \mathbf{M}_i)(\mathbf{r}_{ij} \cdot \mathbf{M}_j) r_{ij}^{-5}] = -\frac{\mu_0}{2} \sum_i \mathbf{M}_i \cdot \mathbf{B}_i^{\text{dip}}, \quad (1)$$

where $r_{ij} = |\mathbf{r}_{ij}| = |\mathbf{r}_i - \mathbf{r}_j|$ is the distance between the centers of particles i and j , and μ_0 the vacuum

permeability. The infinite range of the dipole interaction is taken into account by applying an Ewald-type summation over all periodically arranged unit cells of the extended thin film [20]. In addition to the usual point-dipole sum we consider the leading correction resulting from the finite particle size (dipole-quadrupole interaction), which is outlined in detail in the Appendix. This correction becomes comparable to the point-dipole sum for large particle coverages or small interparticle distances. The energy unit of the dipole coupling is given by $E_{\text{dip}}^0 = \mu_{\text{at}}^2/a_0^3$, with μ_{at} in units of the Bohr magneton μ_B . In this study we assume values appropriate to Fe ($\mu_{\text{at}} = 2.2 \mu_B$, $a_0 = 2.5 \text{ \AA}$), which yields $E_{\text{dip}}^0 = 0.19 \text{ K}$. The effects of single-particle anisotropies resulting from the spin-orbit interaction, the dipole interaction among atomic magnetic moments within each particle (shape anisotropy), external magnetic fields, and finite temperatures are beyond the scope of the present study.

Starting from an arbitrary initial configuration $\{\phi_i^{\text{initial}}\}$ of the magnetic directions, the total magnetic energy E_{dip} of the system is relaxed to the nearest local minimum, which often corresponds to a metastable state, by varying all in-plane angles ϕ_i of the particles using a conjugated gradient method [21]. For example, the experimental situation of a remanent state after removal of an external magnetic field is simulated by choosing a fully aligned initial arrangement along a certain direction. We emphasize that the applied procedure is not intended to search preferently for the global energy minimum or ground state, which is the equilibrium state at $T = 0$. Rather, at first we determine the energy distribution of the local minima for different degrees of structural disorder introduced in the planar particle array. A number of randomly chosen initial configurations $\{\phi_i^{\text{initial}}\}$ is created and relaxed to a nearby local minimum. This metastable state is characterized by its energy E_{dip} and by its set of angles $\{\phi_i\}$. A twofold (uniaxial) symmetry is always present due to time inversion symmetry, i.e., the energy of a state does not change under the transformation $\phi_i \rightarrow \phi_i + 180^\circ$ performed simultaneously for all particles. These mirrored states are considered to be equivalent. The numbers of trials yielding relaxed states with energies falling into given energy intervals are monitored, and the corresponding energy histogram is determined. Since the minimization procedure relaxes typically to the local energy minimum that is closest to the initial state, this frequency provides a measure of the *catchment area*, i.e., the area of the 'energy valley' belonging to that state in the high-dimensional configuration space.

In order to account for the large number of local energy minima occurring in particle arrangements with structural inhomogeneities we determine the *average dipole energy* $\overline{E}_{\text{dip}}$ resulting from many different trials for the same particle array. In addition, we average $\overline{E}_{\text{dip}}$ over a number of different realizations of the unit cell, using the same global variables which characterize the particle ensemble (coverage, standard deviation σ_R , etc.). For comparison, $\overline{E}_{\text{dip}}$ is also calculated for the same spatial setup by assuming a ferromagnetic state (i.e., $\phi_i = \phi_{\text{fm}}$) and averaging over the FM angle ϕ_{fm} . In case of a disturbed (quasi-periodic) square lattice, i.e., if the particle numbering allows for the identification of a square plaquette of four neighbouring particles, we also determine the dipole energy for the microvortex magnetic arrangement, averaging over the MV angle ϕ_{mv} . Note that for a nonuniform particle ensemble these FM and MV magnetic arrangements do not correspond in general to local energy minima. For a *random* set of angles $\{\phi_i\}$ one obtains $\overline{E}_{\text{dip}} = 0$ which constitutes the

natural energy reference.

The deviations of the metastable low-energy magnetic arrangements from the MV state are quantified by the *global* and *local microvortex order parameters* $M_{\text{mv}}^{\text{global}}(\sigma_R)$ and $M_{\text{mv}}^{\text{local}}(\sigma_R)$ given by

$$M_{\text{mv}}^{\text{global}}(\sigma_R) = \frac{1}{n} \left[\left(\sum_i^n (-1)^{i_y} \cos \phi_i \right)^2 + \left(\sum_i^n (-1)^{i_x} \sin \phi_i \right)^2 \right]^{1/2}, \quad (2)$$

$$M_{\text{mv}}^{\text{local}}(\sigma_R) = \frac{1}{4} \left[\left(\sum_i^4 (-1)^{i_y} \cos \phi_i \right)^2 + \left(\sum_i^4 (-1)^{i_x} \sin \phi_i \right)^2 \right]^{1/2}, \quad (3)$$

where i_y and i_x denote the numbering of the rows and columns corresponding to particle i . Clearly, a reference square lattice is prerequisite. Hence, we restrict ourselves to a quasi-periodic array or to a square array with vacancies for which i_y and i_x can be uniquely defined. These two order parameters differ by the sum i running either over all n particles of the unit cell or over the four neighbouring particles within a square plaquette. They have a simple geometrical interpretation as the projection of the magnetic configuration on the two linear independent columnar states having $\phi_{\text{mv}} = 0^\circ$ and $\phi_{\text{mv}} = 90^\circ$, regardless of all possible rotations of the MV states within this plane. $M_{\text{mv}}^{\text{global}}(\sigma_R)$ measures the MV order in the nanostructure, whereas $M_{\text{mv}}^{\text{local}}(\sigma_R)$ measures the short range ordering. Both quantities are averaged over an appropriate number of initial configurations for the same particle arrangement and over different realizations of the unit cell. In addition $M_{\text{mv}}^{\text{local}}(\sigma_R)$ is averaged over all four-particle plaquettes within the unit cell.

Finally, another quantity characterizing the magnetic properties of nanostructured particle arrangements is the distribution of the microvortex angles ϕ_{mv} . Prakash and Henley observed that the preferred MV angles for a square particle array with a small number of randomly distributed vacancies are the diagonal directions ($\phi_{\text{mv}} = 45^\circ, 135^\circ$, etc.) [10]. It is therefore interesting to investigate how the angular distribution of the microvortex angles depends on the type and degree of disorder. For this purpose different realizations of the nanostructure are created. For each particle setup the MV state with angle ϕ_{mv} yielding the lowest energy is determined, and the corresponding frequencies for all angles are monitored. We consider a *disturbed* square particle array with standard deviation σ_R , and a *diluted* square particle lattice with a concentration C_{vac} of vacancies. It should be noted that for a small number of vacancies one obtains an appreciable dependence on the shape of the unit cell (aspect ratio of the rectangle), since these vacancies are located effectively on a square or rectangular lattice due to the periodic boundary conditions.

3. Results

First, figure 1 illustrates some representative low-energy magnetic arrangements of disordered particle arrays. With increasing disorder, characterized by the positional standard deviation σ_R , the magnetic configurations of the relaxed solutions become increasingly noncollinear. Results are given for the magnetic states of a slightly disturbed ($\sigma_R/R_0 = 0.05$), a moderately disturbed ($\sigma_R/R_0 = 0.10$),

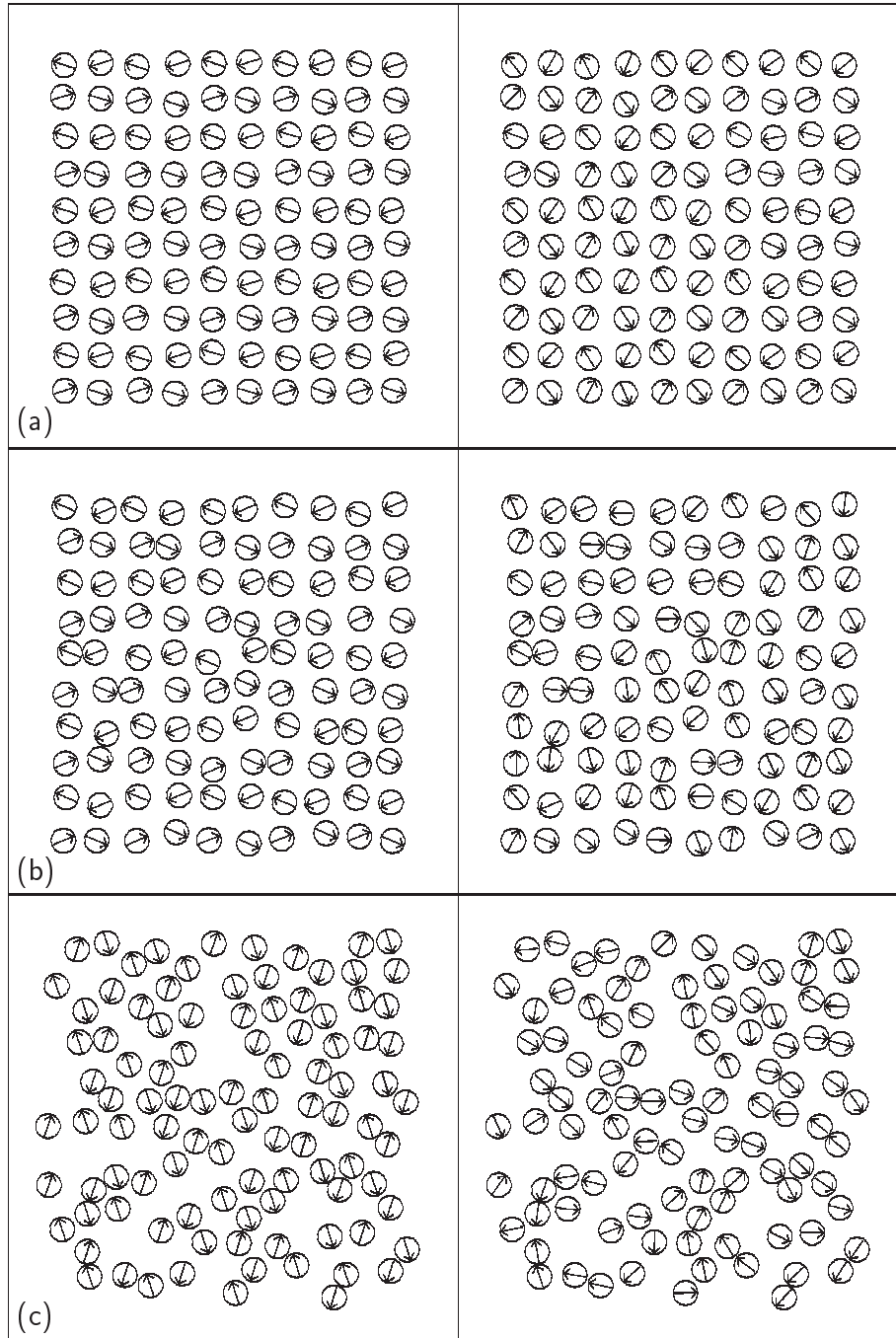


Figure 1. Illustrations of the magnetic arrangements in two-dimensional nanostructures. The particle positions are scattered around the lattice sites of a square array with positional standard deviations (a) $\sigma_R/R_0 = 0.05$, (b) $\sigma_R/R_0 = 0.1$, and (c) $\sigma_R/R_0 = 0.5$, where R_0 refers to the average interparticle distance. The surface coverage amounts to $C = 35\%$. The left columns refers to microvortex magnetic arrangements. Relaxation of the magnetic moment directions using these arrangements as starting configurations yields the metastable solutions shown in the right columns.

and a strongly disturbed ($\sigma_R/R_0 = 0.50$) particle setup having all the same coverage $C = 35$ %. Both the optimal microvortex states and the relaxed solutions are shown. For $\sigma_R/R_0 = 0.05$ the MV arrangement resembles quite closely the true solution, see figure 1(a). However, as can be seen in figure 1(b), already a moderate amount of positional disorder destroys the MV state. This is physically reasonable since the MV order is tightly connected to the presence of a square-lattice symmetry of the particle ensemble. The degree of the MV ordering will be quantified below. For large σ_R or for a random particle setup the resulting magnetic arrangement is dominated by the formation of chains and loops of magnetic moments with a correlated ‘head-to-tail’ alignment of the particle magnetizations, see figure 1(c) [22]. This reflects the tendency of the dipole interaction to favour a locally demagnetized state with a vanishing or small net magnetization.

In figure 2 we present examples for the dipole energy distribution of metastable states of slightly and moderately disturbed particle setups shown in figures 1(a) and (b). These were obtained by considering 20000 random initial configurations $\{\phi_i^{\text{initial}}\}$ and by assigning the energies of the relaxed states to energy intervals $[E, E + \Delta E]$, with $\Delta E = 5 \cdot 10^{-3}$ K. Distinctly different energy distributions are observed for weak and strong disorder. For weak disorder [e.g., $\sigma_R/R_0 = 0.05$, see figure 2(a)] an *asymmetric* energy distribution is found. The lowest energy state is reached very often, in fact about 50 % of the trials relax to that ground state for $\sigma_R/R_0 = 0.03$, and about 30 % for $\sigma_R/R_0 = 0.05$. Moreover, the ground state configuration resembles closely the MV state with an almost vanishing net magnetization. In addition, numerous metastable states are obtained, which energies are distributed over a relatively broad range, and which are reached far less frequently. In other words, for weak disturbances the catchment area of the ground state is much larger than the ones of the higher-energy states. It is interesting to note that the energy differences between the few states with the lowest energies are quite larger than those found for less stable magnetic arrangements. Since these latter states often exhibit a finite net magnetization, one expects that an external magnetic field tends to stabilize these higher-energy metastable configurations.

Already for moderate disorder $\sigma_R/R_0 = 0.10$ the character of the energy distribution changes strongly. An almost *symmetric*, Gaussian-like energy distribution is obtained around the average dipole energy $\overline{E}_{\text{dip}}$, see figure 2(b). The number of metastable states has increased remarkably. In fact, out of the considered 20000 random trials no single state is reached twice after relaxation. This is in particular true for the low-energy states which are obtained with a very small frequency [see the encircled region in figure 2(b)]. For an even stronger disorder the small peak in the frequency distribution for the low-energy states disappears completely. Since the total number of metastable states increases strongly with increasing disorder, the corresponding catchment areas decreases dramatically. The obtained large number of metastable states is consistent with experiments on ferrofluids, which show that after application and removal of an external magnetic field the same magnetic arrangement is seldomly reached for a second time [23].

Furthermore, from figure 2 one observes clearly that the average magnetic dipole energy $\overline{E}_{\text{dip}}$ decreases with increasing positional standard deviation σ_R . In figure 3 we present results for

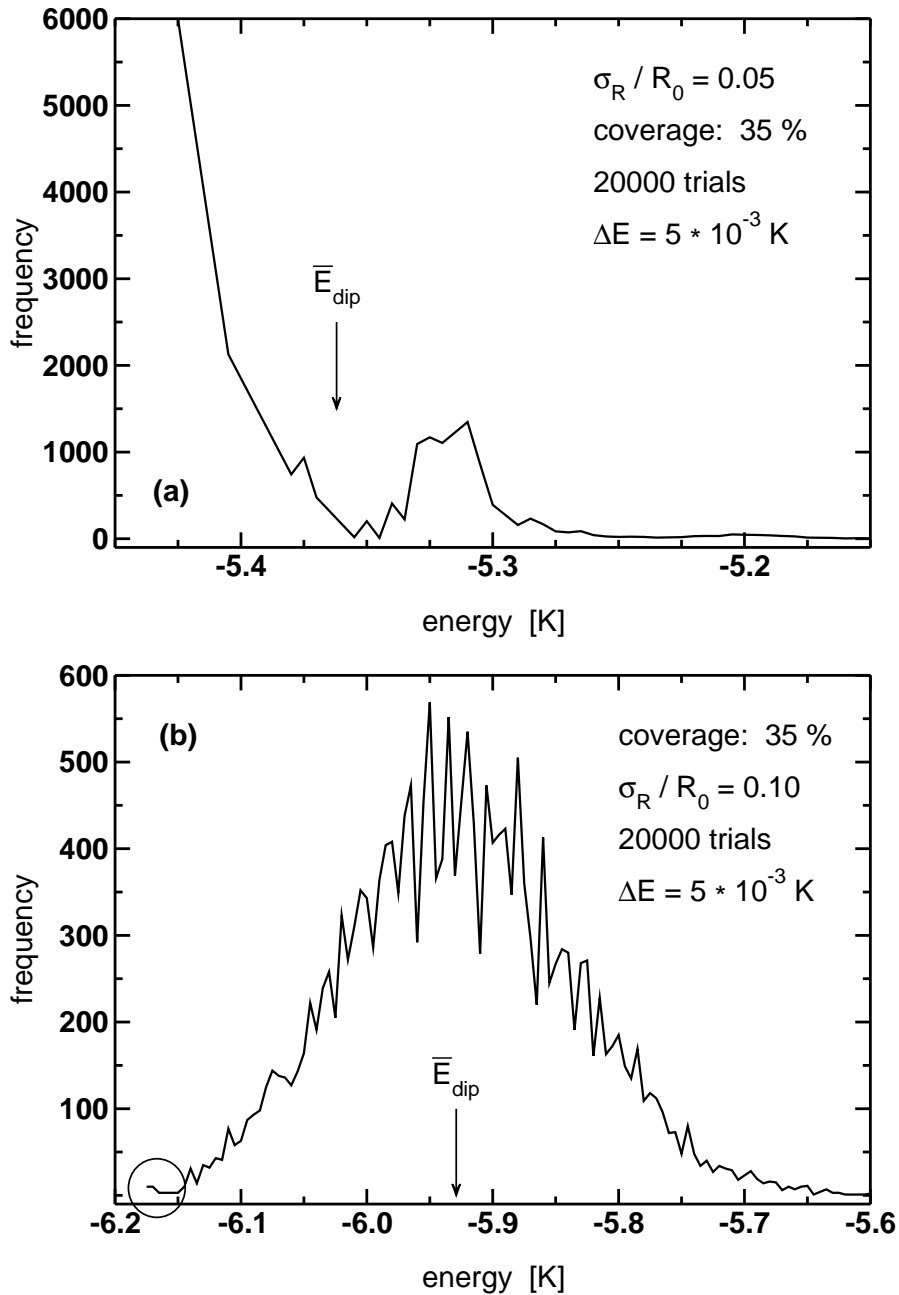


Figure 2. Energy distribution of local energy minima for two disturbed square particle arrays using different positional standard deviations (a) $\sigma_R/R_0 = 0.05$, and (b) $\sigma_R/R_0 = 0.10$. The particle coverage amounts to $C = 35\%$. The distributions of the metastable states are obtained from 20000 randomly chosen initial configurations and sampled into energy intervals with width $\Delta E = 5 \cdot 10^{-3}$ K. Also indicated is the resulting average dipole energy $\bar{E}_{\text{dip}}(\sigma_R)$.

$\bar{E}_{\text{dip}}(\sigma_R, C)$ per particle as function of σ_R and for different particle coverages C . A square lattice corresponds to $\sigma_R = 0$. Results for random particle setups are also shown. $\bar{E}_{\text{dip}}(\sigma_R)$ is calculated for the relaxed solutions as well as for the ferromagnetic and microvortex magnetic states averaged

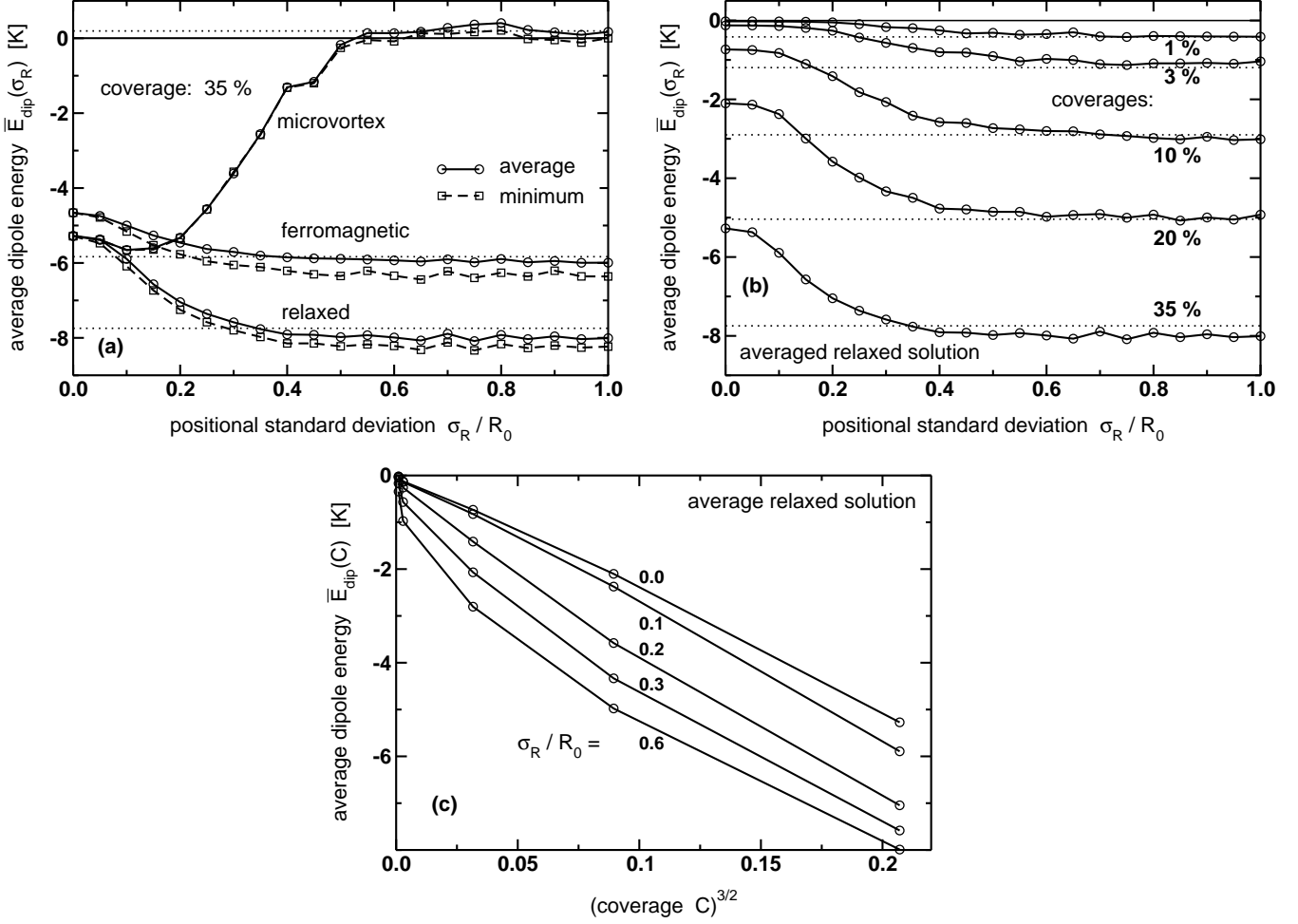


Figure 3. (a) Average dipole energy $\overline{E}_{\text{dip}}(\sigma_R)$ per particle of a planar array of magnetic particles as function of the positional standard deviation σ_R . R_0 refers to the average interparticle distance, and the coverage amounts to $C = 35\%$. Displayed are $\overline{E}_{\text{dip}}(\sigma_R)$ for the relaxed magnetic states, averaged over 40 different initial conditions (full lines, circles), and the minimum energies (dashed lines, squares) which indicate the dispersion of the data. Results are also given for the ferromagnetic and microvortex magnetic arrangements, averaged over the in-plane angles. The dotted lines denote $\overline{E}_{\text{dip}}$ for a random particle setup with same particle sizes and coverages. All results correspond to the average over 20 different realizations of the unit cell.

(b) $\overline{E}_{\text{dip}}(\sigma_R, C)$ of relaxed magnetic arrangements as function of σ_R for different coverages C as indicated. The dotted lines denote $\overline{E}_{\text{dip}}(C)$ for random particle setups.

(c) $\overline{E}_{\text{dip}}(\sigma_R, C)$ of relaxed magnetic arrangements as function of the particle coverage C for different σ_R as indicated. We show $\overline{E}_{\text{dip}}(C)$ as function of $C^{-3/2}$ which should yield a linear behaviour from a simple scaling estimate.

over the corresponding in-plane angles ϕ_{fm} and ϕ_{mv} . The obtained minimum values of $\overline{E}_{\text{dip}}(\sigma_R)$ are also displayed in order to illustrate the spread of the results around the average. Whereas the energy distributions shown in figure 2 are determined from a *single* realization of the unit cell, here $\overline{E}_{\text{dip}}(\sigma_R)$ is in addition averaged over 20 different realizations.

In figure 3(a), $\overline{E}_{\text{dip}}(\sigma_R)$ is shown for a coverage $C = 35\%$. With increasing σ_R the average dipole energy *decreases*, i.e., the respective magnetic binding energy *increases* with *increasing disorder* [24]. For $\sigma_R/R_0 \gtrsim 0.5$, $\overline{E}_{\text{dip}}(\sigma_R)$ approaches a constant value which corresponds, within the numerical dispersion of the data, to the average dipole energy for a *random* particle array. The decrease of the average energy is caused by the nonlinear dependence of the dipole interaction with respect to the interparticle distance [24]. In fact, once disorder is introduced, the increase of $\overline{E}_{\text{dip}}$ for enlarged distances r_{ij} between some particle pairs is more than counterbalanced by a corresponding decrease for smaller distances between other pairs of particles. A similar behaviour is obtained for the ferromagnetic arrangement, albeit with a larger $\overline{E}_{\text{dip}}(\sigma_R)$. In contrast, for the MV state the average energy exhibits a minimum as function of σ_R at $\sigma_R/R_0 \sim 0.15$, and approaches $\overline{E}_{\text{dip}} = 0$ with increasing σ_R . Relaxation in a disordered particle arrangement, see figure 1, is thus crucial to the disorder induced reduction of $\overline{E}_{\text{dip}}(\sigma_R)$. Let us recall that the FM and MV arrangements usually do not correspond to local energy minima for $\sigma_R > 0$.

In figure 3(b) we show $\overline{E}_{\text{dip}}(\sigma_R)$ of the relaxed solutions and for different particle coverages C . First of all one observes that the overall dependence of $\overline{E}_{\text{dip}}$ on σ_R is not significantly affected by C . Increasing the interparticle spacing R_0 decreases the magnitude of the average dipole energy, which should scale in principle as $\overline{E}_{\text{dip}} \propto R_0^{-3} \propto C^{3/2}$. The dependence of $\overline{E}_{\text{dip}}$ on C is depicted in figure 3(c) for the relaxed solutions. Indeed, the expected behaviour $\overline{E}_{\text{dip}} \propto C^{3/2}$ is obtained for weak positional disorder σ_R . However, for strong disorder and for small coverages a different concentration dependence is observed. It seems that the strong magnetic noncollinearities of the magnetic configurations render the simple scaling expectation no longer applicable. It would be therefore interesting to investigate in detail the energy scaling as function of coverage C especially in the limit of strongly disturbed arrays of magnetic particles.

Note that the magnitude of the dipole energy is comparably small. This is a consequence of the disk-shaped particles assumed in our calculations. For compact sphere-shaped particles with the same radius r_0 as the disk-shaped ones, thus yielding the same surface coverage C , the corresponding dipole energy will be significantly enhanced due to the larger number of atoms $N = (r_0/a_0)^3$ per spherical particle. Moreover, similar as the positional disorder a particle-size dispersion yields noncollinear magnetic arrangements even if the particle centers form a periodic lattice. However, one observes that $\overline{E}_{\text{dip}}$ does not vary strongly with increasing size dispersion [25].

Furthermore, we discuss the crossover from a quasi-periodic to a random particle ensemble. In figure 4 we show the coverage dependence of the positional standard deviation $\overline{\sigma}_R$, above which the average energy $\overline{E}_{\text{dip}}(\sigma_R)$ of a quasi-periodic particle arrangement reaches the limiting value of a random setup. One observes that $\overline{\sigma}_R$ decreases with increasing coverage C , as can qualitatively be explained by the following simple scaling consideration. The particles are scattered within a certain distance around the sites of the square lattice, the average scattering radius R_{σ_R} can be estimated by $R_{\sigma_R} \simeq \sigma_R R_0$. For a given coverage C the average dipole energy for a random particle setup is approximately reached for the *crossover standard deviation* $\overline{\sigma}_R$ for which R_{σ_R} plus the particle

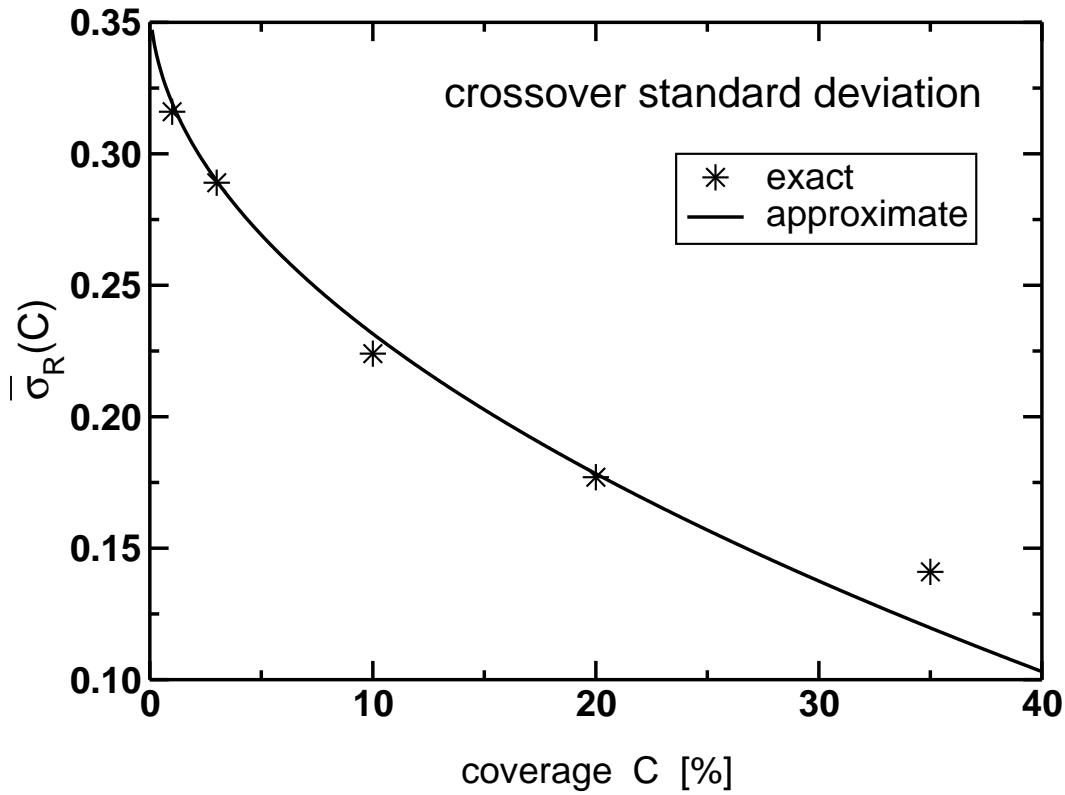


Figure 4. Crossover standard deviation $\bar{\sigma}_R$ as function of the coverage C . For $\sigma_R > \bar{\sigma}_R$ the average dipole energy per particle $\bar{E}_{\text{dip}}(\sigma_R)$ of a disturbed square particle array converges to the one of a random particle setup. The symbols refer to the inflection points of $\bar{E}_{\text{dip}}(\sigma_R)$ extracted from figure 3(b), and the full line to equation 5 using 0.72 as proportionality factor.

radius equals half of the average interparticle distance,

$$R_{\bar{\sigma}_R} + r_0 \simeq R_0/2. \quad (4)$$

Using $C = \pi(r_0/R_0)^2$, one obtains

$$\bar{\sigma}_R(C) \simeq \frac{1}{2} - \sqrt{\frac{C}{\pi}}. \quad (5)$$

In figure 4, $\bar{\sigma}_R(C)$ is compared with the inflection points of $\bar{E}_{\text{dip}}(\sigma_R)$ extracted from figure 3(b) for various coverages C . One observes that except for the largest considered coverage $C = 35\%$ a satisfactory agreement is obtained, which supports the validity of the previous scaling considerations.

Results for the global and local microvortex order parameters $M_{\text{mv}}^{\text{global}}(\sigma_R)$ and $M_{\text{mv}}^{\text{local}}(\sigma_R)$ are presented in figure 5, assuming two different types of disorder. In figure 5(a) we consider a disturbed square particle lattice as function of the positional standard deviation σ_R for a coverage $C = 35\%$,

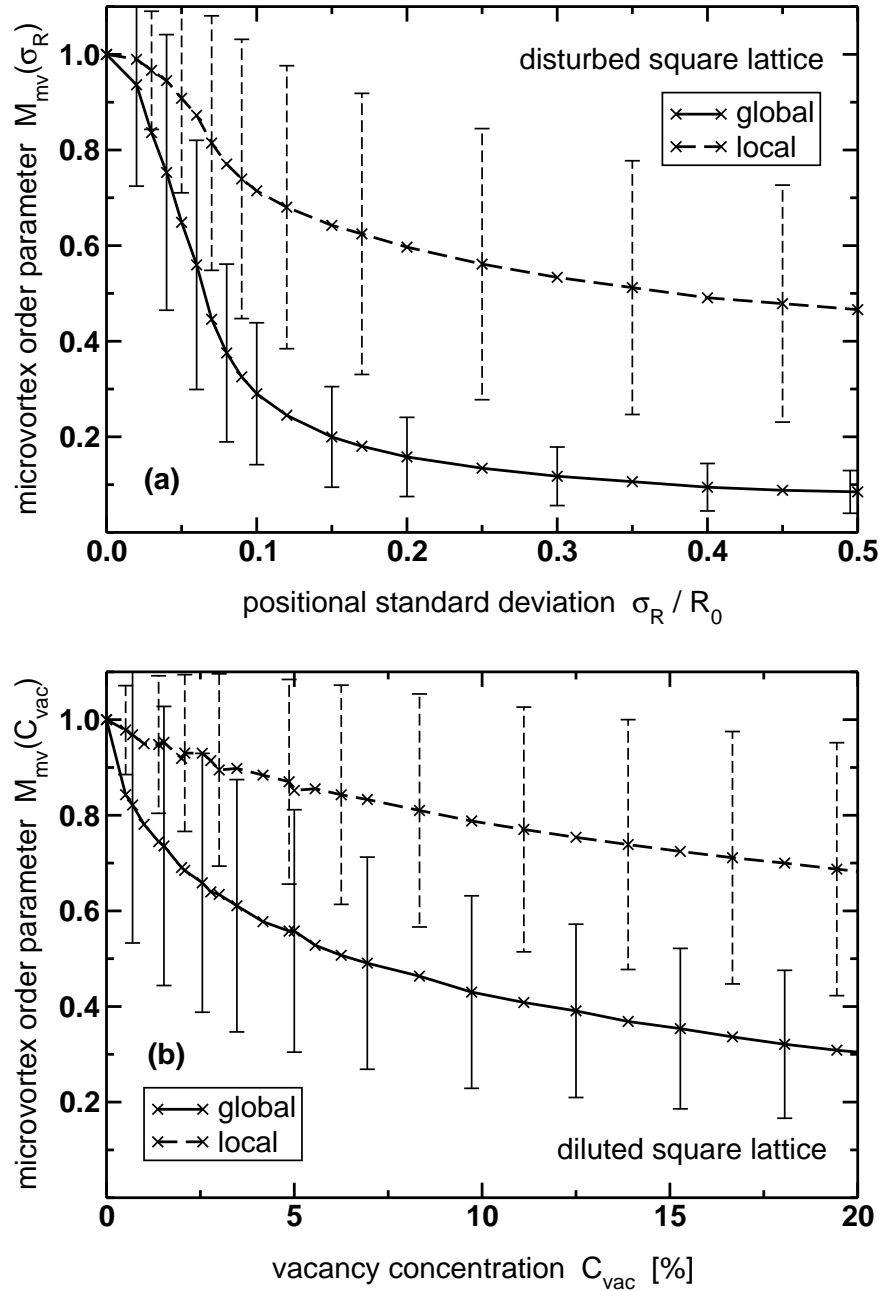


Figure 5. Global and local microvortex order parameters $M_{mv}^{\text{global}}(\sigma_R)$ and $M_{mv}^{\text{local}}(\sigma_R)$ as function of the distortion of the particle array assuming (a) a disturbed square lattice with positional standard deviation σ_R and particle coverage $C = 35$ %, and (b) a square array with randomly distributed vacancies with concentration C_{vac} . These order parameters are averaged over many different initial arrangements and different realizations of the unit cell, in addition $M_{mv}^{\text{local}}(\sigma_R)$ is averaged over all four-particle plaquettes in the unit cell. The resulting standard deviation is indicated by the error bars.

and in figure 5(b) we vary the concentration of vacancies in an otherwise periodic array. The rather large dispersions of the MV order parameters result from many different initial arrangements and different realizations of the unit cell. Locally the MV order is preserved even for strong disorder. For example, for $\sigma_R/R_0 = 0.5$ which refers to an almost random particle array, see figure 3(a), we obtain $M_{\text{mv}}^{\text{local}} \sim 0.5$, and $M_{\text{mv}}^{\text{local}} \sim 0.7$ for $C_{\text{vac}} = 20\%$. In contrast, positional disorder has a much stronger effect on $M_{\text{mv}}^{\text{global}}$. Especially positional disturbances quickly destroy the long-range MV ordering in the square lattice. For instance, for a particle coverage $C = 35\%$ this occurs already for $\sigma_R/R_0 \gtrsim 0.10$, which is consistent with the minimum of $\overline{E}_{\text{dip}}(\sigma_R)$ of the MV state, see figure 3(a).

Finally, we present results for the angular distribution of the microvortex angle ϕ_{mv} for different degrees of disorder. We consider first the effect of *vacancies* in an otherwise periodic square particle lattice, as has been done previously by Prakash and Henley [10]. According to these authors the preferred MV angles for a dipole-coupled square spin lattice with a small amount of vacancies correspond to the diagonal directions. Indeed, as can be seen from figure 6, a strong frequency of the diagonal MV angles $\phi_{\text{mv}} = 45^\circ$ and 135° is obtained for low vacancy concentrations C_{vac} . The frequencies of these states decrease with increasing C_{vac} , and vanish for $C_{\text{vac}} \gtrsim 6 - 7\%$. In addition to the diagonal states we also obtain a strong frequency of the MV angle along the axial directions (columnar states) with MV angles $\phi_{\text{mv}} = 0^\circ$, 90° , and 180° . These states are also present for larger vacancy concentrations. We have investigated whether the angular distributions are affected by the finite size of the unit cell, in particular whether this could induce the pronounced frequencies of the columnar states. If this is true, the ratio of the frequencies of $\phi_{\text{mv}} = 0^\circ$ and $\phi_{\text{mv}} = 90^\circ$ is affected by a variation of the aspect ratio of the rectangular unit cell. We found that for not too small C_{vac} the dependence of the calculated frequencies for columnar and diagonal states as function of size and shape of the unit cell is quite weak. Hence, our results indicate that the presence of a few vacancies induces a more complicated angular distribution of the MV angle. In any case, we would like to point out that at present we cannot rule out completely the possibility that the pronounced frequencies of the columnar states might be caused by the finite size of the unit cell.

Concerning other types of disorder, we observe that for a *disturbed* square lattice characterized by the positional standard deviation σ_R there is no particular preference of the diagonal states. For this type of disorder only the columnar states exhibit a pronounced frequency as compared to the rest of the MV angles. The frequency peaks for columnar states decrease for increasing disorder and vanish above $\sigma_R/R_0 \sim 0.20$ for the particle coverage $C = 35\%$. A marked dependence of the angular distribution on the size and shape of the unit cell is not observed also for this type of disorder. To conclude this discussion, we would like to emphasize that the angular distributions presented in figure 6 were all obtained for a *nonrelaxed* MV state. We have also performed corresponding calculations for the *relaxed* solutions, and have determined the MV states which are closest to the noncollinear relaxed magnetic arrangements. In contrast to the results shown in figure 6 the corresponding angular histograms for the relaxed states exhibit a strong dependence on the size and shape of the unit cell. Therefore, further investigations would be necessary in order to clarify this matter.

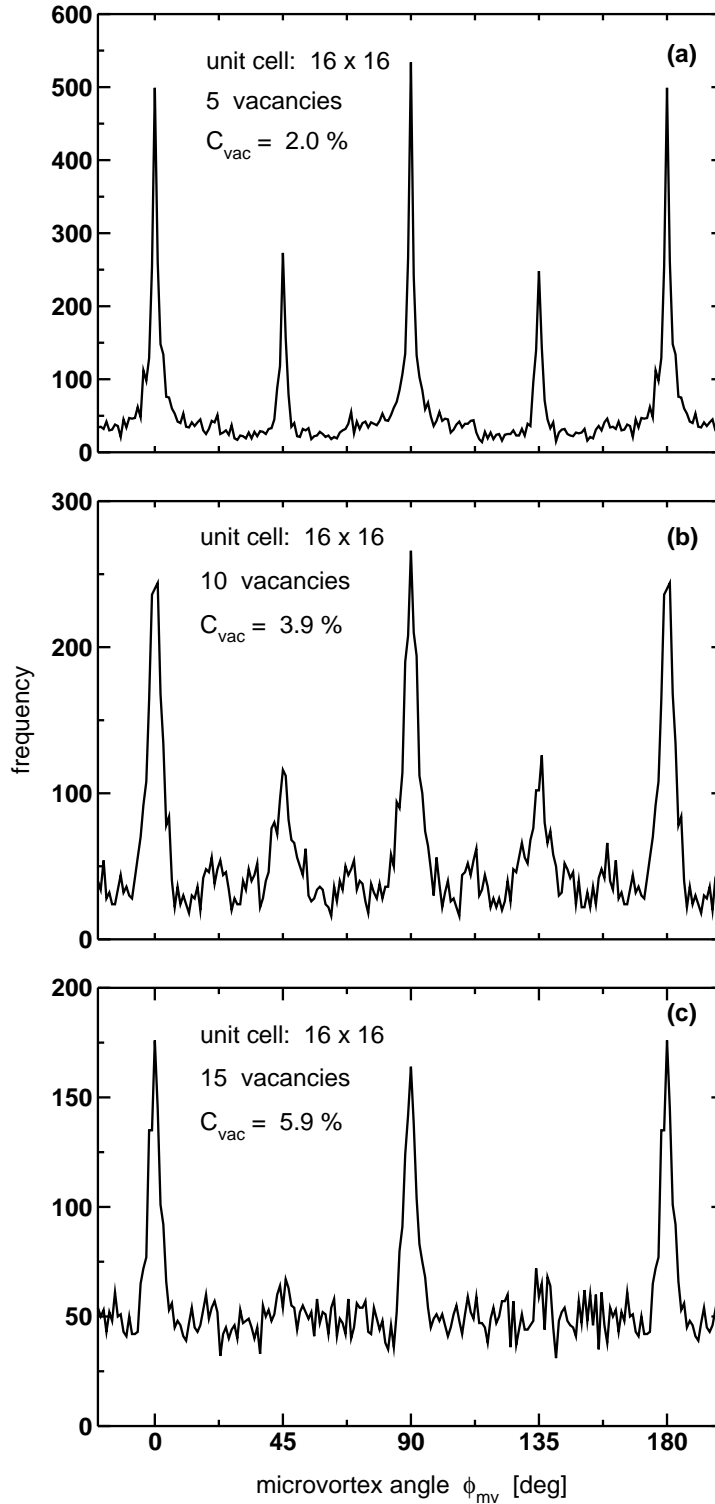


Figure 6. Angular distribution of the microvortex angle ϕ_{mv} for different vacancy concentrations C_{vac} on a square lattice. (a) $C_{vac} = 2.0\%$ (5 vacancies per unit cell), (b) $C_{vac} = 3.9\%$ (10 vacancies), and (c) $C_{vac} = 5.9\%$ (15 vacancies). The size of the unit cell is 16×16 particles, 1000 different realizations of the unit cell are performed. Due to the mirror symmetry we show the angular distribution for $-20^\circ \leq \phi_{mv} \leq 200^\circ$.

4. Conclusion

In the present study we have investigated the low-energy properties of disordered planar arrays of magnetic nanoparticles interacting by the dipole coupling. Different kinds of disorder have been considered. Already small deviations from a square particle lattice lift the continuous degeneracy of the microvortex ground state. A strongly noncollinear magnetic order appears in the nanostructure which destroys the MV arrangement, as can be seen from the corresponding order parameter. We have shown that with an increasing disorder the energy distribution of the metastable states changes qualitatively. Our results indicate that it should be very difficult to identify the ground state energy and its magnetic configuration for strongly inhomogeneous particle arrangements. This behaviour is typical for spin-glass systems or random magnets. A detailed investigation of the spin-glass behaviour of the nanostructure is certainly worthwhile. This would require the consideration of additional properties such as the nonlinear susceptibility and the time dependent correlation functions [3, 17].

It has been shown that the average magnetic dipole energy of an ensemble of magnetic particles decreases with increasing positional disorder. Moreover, the average dipole energy $\overline{E}_{\text{dip}}$ of a quasi-periodic particle arrangement resembles the one of a random particle setup above the coverage-dependent crossover standard deviation $\overline{\sigma}_R(C)$. A simple scaling behaviour of $\overline{\sigma}_R(C)$ has been derived, which reproduces quite accurately the coverage dependence of $\overline{\sigma}_R(C)$. Structural disorder and strong magnetic noncollinearity effects result in a deviation from the straightforward scaling $\overline{E}_{\text{dip}} \propto C^{3/2}$ of the average dipole energy as function of the coverage.

For a square particle lattice with a small vacancy concentration we found a preferred orientation of the microvortex angle ϕ_{mv} along the diagonal directions. This is in agreement with the results obtained previously by Prakash and Henley [10]. The pronounced frequency of this state decreases with an increasing vacancy concentration. However, we also find indications that the columnar states are particularly frequent. The difference with previous results could be related to the fact that isolated vacancies were considered in [10], whereas in the present study the vacancy concentration cannot be chosen arbitrarily small. In contrast to the case of vacancy-induced disorder, for a disturbed square particle array characterized by the positional standard deviation σ_R a pronounced frequency is found only for the columnar but not for the diagonal states.

The determination of $\overline{E}_{\text{dip}}$ allows to distinguish whether a magnetic particle ensemble can be considered as a weakly or a strongly interacting system. In the first case the interactions can be treated as perturbations to the single-particle couplings, whereas in the latter case they have to be considered explicitly. The present study can be easily extended in order to take into account single-particle anisotropies with distributions of their magnitudes and easy axes. The importance of collectively ordered magnetic states for strongly interacting particle systems has been pointed out. An increasing average binding energy $|\overline{E}_{\text{dip}}|$ favours magnetic ordering and should cause an increase of its critical spin-glass temperature. In this context the effect of disorder in the particle ensemble on the critical temperature is of considerable interest. Also the magnetic relaxation will depend

sensitively on the degree of disorder in such nanostructured systems. Finite temperature effects can be introduced in the framework of a mean field approximation or by performing Monte Carlo simulations. Magnetic hysteresis loops and susceptibilities can be derived by applying magnetic fields with different directions and strengths.

Acknowledgments

The authors acknowledge support from CNRS (France) and from the EU GROWTH project AMMARE (contract number G5RD-CT-2001-00478). We thank P. Politi for fruitful discussions and for sending us his work prior to publication.

Appendix A. Dipole interaction between magnetic particles with a finite size

In this Appendix we determine the leading correction to the magnetic dipole interaction, see equation 1, beyond the point-dipole sum. The finite extension of the particles for the most general case of arbitrary sizes and shapes is taken into account. For a hexagonal lattice the finite particle size has been considered already by Politi and Pini [12]. First, the interaction between a particle pair is calculated. Then a particle ensemble with an infinite lateral extension is modeled by means of a rectangular unit cell with periodic boundary conditions.

The dipole-quadrupole correction

Consider a particle i containing N_i atoms on lattice sites k with position vectors $\mathbf{r}_{ik} = \mathbf{r}_{i0} + \mathbf{r}_k$. The center of gravity of this particle is given by

$$\mathbf{r}_{i0} = (x_{i0}, y_{i0}, z_{i0}) = \frac{1}{N_i} \sum_{k \in i} \mathbf{r}_{ik} = \frac{1}{N_i} \sum_{k \in i} (x_{ik}, y_{ik}, z_{ik}). \quad (\text{A.1})$$

The finite size of particle i is taken into account by the quadratic deviations with respect to its center,

$$\langle x_i^2 \rangle = \frac{1}{N_i} \sum_{k \in i} x_k^2 = \frac{1}{N_i} \sum_{k \in i} (x_{ik} - x_{i0})^2, \quad (\text{A.2})$$

and similarly for $\langle y_i^2 \rangle$ and $\langle z_i^2 \rangle$. These quantities depend on the size and shape of the particle and have the dimension of an area. Furthermore, we define ε_{ik} by

$$r_{ik}^2 = (x_{i0} + x_k)^2 + (y_{i0} + y_k)^2 + (z_{i0} + z_k)^2 = r_{i0}^2 (1 + \varepsilon_{ik}), \quad (\text{A.3})$$

hence,

$$\varepsilon_{ik} = \frac{1}{r_{i0}^2} \left(2x_{i0}x_k + 2y_{i0}y_k + 2z_{i0}z_k + x_k^2 + y_k^2 + z_k^2 \right), \quad (\text{A.4})$$

with $r_{i0}^2 = x_{i0}^2 + y_{i0}^2 + z_{i0}^2$. The factor $(1 + \varepsilon_{ik})$ appearing in the denominator of the dipole interaction energy, see equation 1, is expanded to second order in x_k , y_k , and z_k as

$$\begin{aligned} \frac{1}{(1 + \varepsilon_{ik})^{5/2}} &\simeq 1 - \frac{5}{2} \varepsilon_{ik} + \frac{35}{8} \varepsilon^2 \simeq \\ 1 - \frac{5}{2r_{i0}^2} \left(2x_{i0}x_k + 2y_{i0}y_k + 2z_{i0}z_k + x_k^2 + y_k^2 + z_k^2 \right) &+ \frac{35}{2r_{i0}^4} \left(x_{i0}x_k + y_{i0}y_k + z_{i0}z_k \right)^2. \end{aligned} \quad (\text{A.5})$$

Now all different sums over the atomic sites k of particle i are performed up to this order. The non-vanishing terms are listed in the following equations A.6–A.15.

$$\begin{aligned} \sum_{k \in i} \frac{1}{r_{ik}^5} &= \sum_{k \in i} \frac{1}{r_{i0}^5 (1 + \varepsilon)^{5/2}} \\ &\simeq \frac{N_i}{r_{i0}^5} + \frac{5N_i}{2r_{i0}^7} \left[\left(7 \frac{x_{i0}^2}{r_{i0}^2} - 1 \right) \langle x_i^2 \rangle + \left(7 \frac{y_{i0}^2}{r_{i0}^2} - 1 \right) \langle y_i^2 \rangle + \left(7 \frac{z_{i0}^2}{r_{i0}^2} - 1 \right) \langle z_i^2 \rangle \right], \end{aligned} \quad (\text{A.6})$$

$$\begin{aligned} \sum_{k \in i} \frac{x_{ik}}{r_{ik}^5} &= \sum_{k \in i} \frac{x_{i0} + x_k}{r_{i0}^5 (1 + \varepsilon)^{5/2}} \simeq \frac{N_i}{r_{i0}^5} x_{i0} + \frac{5N_i}{2r_{i0}^7} \left[\left(7 \frac{x_{i0}^3}{r_{i0}^2} - 3x_{i0} \right) \langle x_i^2 \rangle \right. \\ &\quad \left. + \left(7 \frac{x_{i0}y_{i0}^2}{r_{i0}^2} - x_{i0} \right) \langle y_i^2 \rangle + \left(7 \frac{x_{i0}z_{i0}^2}{r_{i0}^2} - x_{i0} \right) \langle z_i^2 \rangle \right], \end{aligned} \quad (\text{A.7})$$

$$\begin{aligned} \sum_{k \in i} \frac{y_{ik}}{r_{ik}^5} &= \sum_{k \in i} \frac{y_{i0} + y_k}{r_{i0}^5 (1 + \varepsilon)^{5/2}} \simeq \frac{N_i}{r_{i0}^5} y_{i0} + \frac{5N_i}{2r_{i0}^7} \left[\left(7 \frac{x_{i0}^2 y_{i0}}{r_{i0}^2} - y_{i0} \right) \langle x_i^2 \rangle \right. \\ &\quad \left. + \left(7 \frac{y_{i0}^3}{r_{i0}^2} - 3y_{i0} \right) \langle y_i^2 \rangle + \left(7 \frac{y_{i0}z_{i0}^2}{r_{i0}^2} - y_{i0} \right) \langle z_i^2 \rangle \right], \end{aligned} \quad (\text{A.8})$$

$$\begin{aligned} \sum_{k \in i} \frac{z_{ik}}{r_{ik}^5} &= \sum_{k \in i} \frac{z_{i0} + z_k}{r_{i0}^5 (1 + \varepsilon)^{5/2}} \simeq \frac{N_i}{r_{i0}^5} z_{i0} + \frac{5N_i}{2r_{i0}^7} \left[\left(7 \frac{x_{i0}^2 z_{i0}}{r_{i0}^2} - z_{i0} \right) \langle x_i^2 \rangle \right. \\ &\quad \left. + \left(7 \frac{y_{i0}^2 z_{i0}}{r_{i0}^2} - z_{i0} \right) \langle y_i^2 \rangle + \left(7 \frac{z_{i0}^3}{r_{i0}^2} - 3z_{i0} \right) \langle z_i^2 \rangle \right], \end{aligned} \quad (\text{A.9})$$

$$\begin{aligned} \sum_{k \in i} \frac{x_{ik}^2}{r_{ik}^5} &= \sum_{k \in i} \frac{x_{i0}^2 + 2x_{i0}x_k + x_k^2}{r_{i0}^5 (1 + \varepsilon)^{5/2}} \simeq \frac{N_i}{r_{i0}^5} \left(x_{i0}^2 + \langle x_i \rangle^2 \right) + \frac{5N_i}{2r_{i0}^7} \left[\left(7 \frac{x_{i0}^4}{r_{i0}^2} - 5x_{i0}^2 \right) \langle x_i^2 \rangle \right. \\ &\quad \left. + \left(7 \frac{x_{i0}^2 y_{i0}^2}{r_{i0}^2} - x_{i0}^2 \right) \langle y_i^2 \rangle + \left(7 \frac{x_{i0}^2 z_{i0}^2}{r_{i0}^2} - x_{i0}^2 \right) \langle z_i^2 \rangle \right], \end{aligned} \quad (\text{A.10})$$

$$\begin{aligned} \sum_{k \in i} \frac{y_{ik}^2}{r_{ik}^5} &= \sum_{k \in i} \frac{y_{i0}^2 + 2y_{i0}y_k + y_k^2}{r_{i0}^5 (1 + \varepsilon)^{5/2}} \simeq \frac{N_i}{r_{i0}^5} \left(y_{i0}^2 + \langle y_i \rangle^2 \right) + \frac{5N_i}{2r_{i0}^7} \left[\left(7 \frac{x_{i0}^2 y_{i0}^2}{r_{i0}^2} - y_{i0}^2 \right) \langle x_i^2 \rangle \right. \\ &\quad \left. + \left(7 \frac{y_{i0}^4}{r_{i0}^2} - 5y_{i0}^2 \right) \langle y_i^2 \rangle + \left(7 \frac{y_{i0}^2 z_{i0}^2}{r_{i0}^2} - y_{i0}^2 \right) \langle z_i^2 \rangle \right], \end{aligned} \quad (\text{A.11})$$

$$\begin{aligned} \sum_{k \in i} \frac{z_{ik}^2}{r_{ik}^5} &= \sum_{k \in i} \frac{z_{i0}^2 + 2z_{i0}z_k + z_k^2}{r_{i0}^5(1+\varepsilon)^{5/2}} \simeq \frac{N_i}{r_{i0}^5} \left(z_{i0}^2 + \langle z_i \rangle^2 \right) + \frac{5N_i}{2r_{i0}^7} \left[\left(7 \frac{x_{i0}^2 z_{i0}^2}{r_{i0}^2} - z_{i0}^2 \right) \langle x_i^2 \rangle \right. \\ &\quad \left. + \left(7 \frac{y_{i0}^2 z_{i0}^2}{r_{i0}^2} - z_{i0}^2 \right) \langle y_i^2 \rangle + \left(7 \frac{z_{i0}^4}{r_{i0}^2} - 5z_{i0}^2 \right) \langle z_i^2 \rangle \right], \end{aligned} \quad (\text{A.12})$$

$$\begin{aligned} \sum_{k \in i} \frac{x_{ik} y_{ik}}{r_{ik}^5} &= \sum_{k \in i} \frac{x_{i0} y_{i0} + x_{i0} y_k + x_k y_{i0} + x_k y_k}{r_{i0}^5(1+\varepsilon)^{5/2}} \\ &\simeq \frac{N_i}{r_{i0}^5} x_{i0} y_{i0} + \frac{5N_i}{2r_{i0}^7} \left[\left(7 \frac{x_{i0}^3 y_{i0}}{r_{i0}^2} - 3x_{i0} y_{i0} \right) \langle x_i^2 \rangle \right. \\ &\quad \left. + \left(7 \frac{x_{i0} y_{i0}^3}{r_{i0}^2} - 3x_{i0} y_{i0} \right) \langle y_i^2 \rangle + \left(7 \frac{x_{i0} y_{i0} z_{i0}^2}{r_{i0}^2} - x_{i0} y_{i0} \right) \langle z_i^2 \rangle \right], \end{aligned} \quad (\text{A.13})$$

$$\begin{aligned} \sum_{k \in i} \frac{x_{ik} z_{ik}}{r_{ik}^5} &= \sum_{k \in i} \frac{x_{i0} z_{i0} + x_{i0} z_k + x_k z_{i0} + x_k z_k}{r_{i0}^5(1+\varepsilon)^{5/2}} \\ &\simeq \frac{N_i}{r_{i0}^5} x_{i0} z_{i0} + \frac{5N_i}{2r_{i0}^7} \left[\left(7 \frac{x_{i0}^3 z_{i0}}{r_{i0}^2} - 3x_{i0} z_{i0} \right) \langle x_i^2 \rangle \right. \\ &\quad \left. + \left(7 \frac{x_{i0} y_{i0}^2 z_{i0}}{r_{i0}^2} - x_{i0} z_{i0} \right) \langle y_i^2 \rangle + \left(7 \frac{x_{i0} z_{i0}^3}{r_{i0}^2} - 3x_{i0} z_{i0} \right) \langle z_i^2 \rangle \right], \end{aligned} \quad (\text{A.14})$$

$$\begin{aligned} \sum_{k \in i} \frac{y_{ik} z_{ik}}{r_{ik}^5} &= \sum_{k \in i} \frac{y_{i0} z_{i0} + y_{i0} z_k + y_k z_{i0} + y_k z_k}{r_{i0}^5(1+\varepsilon)^{5/2}} \\ &\simeq \frac{N_i}{r_{i0}^5} y_{i0} z_{i0} + \frac{5N_i}{2r_{i0}^7} \left[\left(7 \frac{x_{i0}^2 y_{i0} z_{i0}}{r_{i0}^2} - y_{i0} z_{i0} \right) \langle x_i^2 \rangle \right. \\ &\quad \left. + \left(7 \frac{y_{i0}^3 z_{i0}}{r_{i0}^2} - 3y_{i0} z_{i0} \right) \langle y_i^2 \rangle + \left(7 \frac{y_{i0} z_{i0}^3}{r_{i0}^2} - 3y_{i0} z_{i0} \right) \langle z_i^2 \rangle \right]. \end{aligned} \quad (\text{A.15})$$

A simple extension of the previous considerations allows to calculate to the same order the corresponding sums involved in the interaction between two extended particles i and j with sizes N_i and N_j . Let $\mathbf{r}_{ij0} = (x_{ij0}, y_{ij0}, z_{ij0})$ denote the relative position vector between the particle centers. The non-vanishing sums in the interaction energy are given by equations A.6–A.15 after the replacements $N_j \rightarrow N_i N_j$, $r_{j0} \rightarrow r_{ij0}$, $x_{j0} \rightarrow x_{ij0}$, $\langle x_j^2 \rangle \rightarrow \langle x_i^2 \rangle + \langle x_j^2 \rangle$, etc., have been performed. Concerning the summation over all atoms k' of particle j , one obtains, for example, for equation A.6,

$$\begin{aligned} \sum_{k \in i} \sum_{k' \in j} \frac{1}{|\mathbf{r}_{ik} - \mathbf{r}_{jk'}|^5} &\simeq N_i N_j \left[\frac{1}{r_{ij0}^5} + \frac{5}{2r_{ij0}^7} \left(7 \frac{x_{ij0}^2}{r_{ij0}^2} - 1 \right) \left(\langle x_i^2 \rangle + \langle x_j^2 \rangle \right) \right. \\ &\quad \left. + \frac{5}{2r_{ij0}^7} \left(7 \frac{y_{ij0}^2}{r_{ij0}^2} - 1 \right) \left(\langle y_i^2 \rangle + \langle y_j^2 \rangle \right) + \frac{5}{2r_{ij0}^7} \left(7 \frac{z_{ij0}^2}{r_{ij0}^2} - 1 \right) \left(\langle z_i^2 \rangle + \langle z_j^2 \rangle \right) \right]. \end{aligned} \quad (\text{A.16})$$

Thus, within this expansion the dipole interaction between particles i and j is expressed in terms of the distance r_{ij0} between their centers and the quadratic deviations $\langle x_i^2 \rangle$, $\langle x_j^2 \rangle$, etc., characterizing the sizes and shapes of the two particles. The point-dipole sum is recovered by setting $\langle x_i^2 \rangle = 0$, etc. The correction to the point-dipole sum is a dipole-quadrupole interaction, being of the order $(\langle x_i^2 \rangle + \langle x_j^2 \rangle)/r_{ij0}^2$, i.e., the ratio of the particle extensions and the square of the interparticle distance.

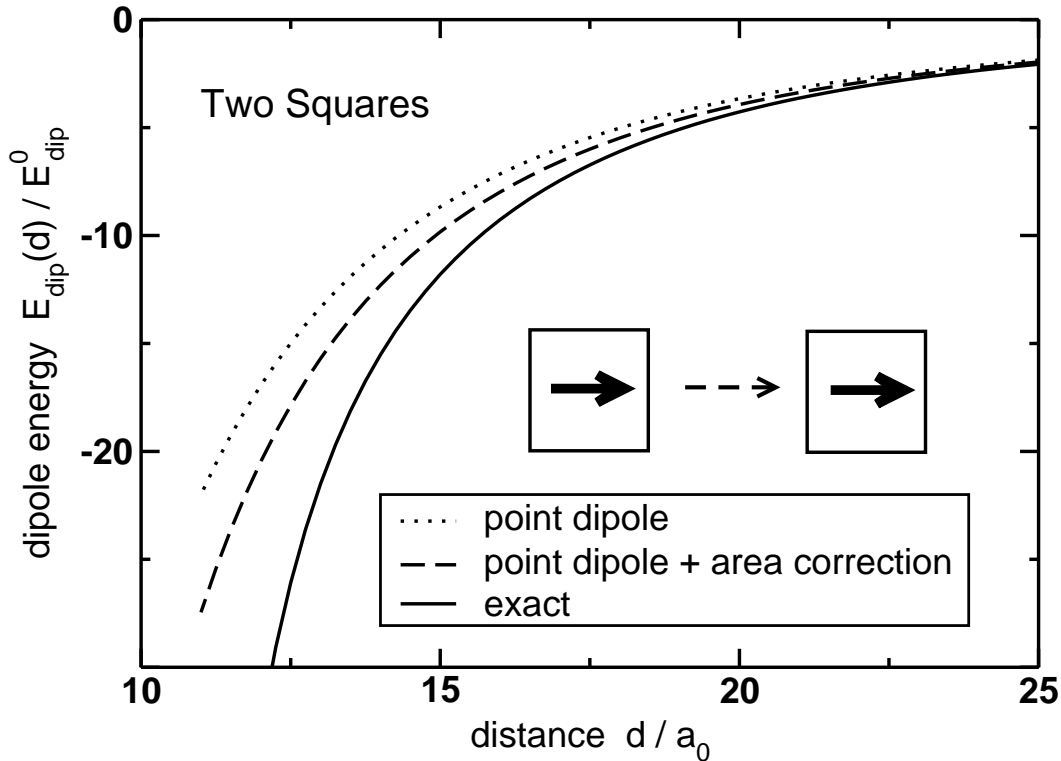


Figure A1. Comparison between the point-dipole approximation, the point-dipole approximation augmented by the dipole-quadrupole correction, and the exactly calculated dipole interaction $E^{\text{dip}}(d)$. We consider two square-shaped flat (001) magnetic particles, consisting of $11 \times 11 = 121$ atomic magnetic moments each. $E_{\text{dip}}(d)$, in units of $E_{\text{dip}}^0 = \mu_{\text{at}}^2/a_0^3$, is shown as function of the distance d between the particle centers in units of the lattice constant a_0 , where μ_{at} is the atomic magnetic moment. Note that for $d/a_0 = 10$ the particles touch each other. The thick arrows illustrate the magnetization directions, which are oriented head-to-tail.

Evidently, the effect of finite particle sizes becomes more important the closer the particles are located. This is the case, for example, for a densely packed 3D ferrofluid or for a layered nanostructured particle ensemble with a large surface coverage.

In figure 7 we compare the exact dipole interaction energy E_{dip} with the results obtained by using the point-dipole approximation with and without the dipole-quadrupole correction. $E_{\text{dip}}(d)$ for two square-shaped particles is shown as function of the distance d between their centers. Notice that the correction for nearby particles amounts to $\sim 25\%$ of the point-dipole sum in this case. For simple particle geometries (e.g., disks, cubes, or spheres) the quadratic deviations $\langle x_i^2 \rangle$, etc., can be calculated analytically. In case of spheres the dipole-quadrupole correction vanishes since a sphere has no quadrupole moment [26].

The extended planar system

Let us now consider a planar particle ensemble infinitely extended in the xy plane. The unit cell has the size $L_x \times L_y$ and consists n particles. Periodic boundary conditions are applied laterally, whereas the vertical extension along the z -direction is finite. The dipole interaction sum runs over all particle pairs within the same and between different unit cells. The position vectors connecting two particle centers are given by $\mathbf{r}_{ij0} = (x_{ij0} + l_x L_x, y_{ij0} + l_y L_y, z_{ij0})$, with l_x and l_y integers. For such a periodic planar system an Ewald summation technique can be applied by using a rapidly convergent 2D lattice summation [20]. The following general sums over the unit cells need to be considered,

$$T_{ij}^{\alpha\beta\gamma} = \sum'_{l_x, l_y = -\infty}^{\infty} \frac{x_{ij0}^\beta y_{ij0}^\gamma}{r_{ij0}^\alpha}. \quad (\text{A.17})$$

The prime at the sum indicates that the term with $r_{ij0} = 0$ is omitted. The different lattice sums appearing in equations A.6–A.15 can be obtained by an appropriate choice of the positive integers α , β , and γ . In general one has to distinguish between the cases $z_{ij0} = 0$ and $z_{ij0} \neq 0$.

The dipole field $\mathbf{B}_i^{\text{dip}}$ of particle i , see equation 1, has the components

$$B_i^{x,\text{dip}} = \mu_{\text{at}} \sum_j N_j \sum'_{l_x, l_y = -\infty}^{\infty} \frac{1}{r^{5/2}} \left[(2x_{ij0}^2 - y_{ij0}^2 - z_{ij0}^2) m_j^x + 3x_{ij0}y_{ij0} m_j^y + 3x_{ij0}z_{ij0} m_j^z \right], \quad (\text{A.18})$$

$$B_i^{y,\text{dip}} = \mu_{\text{at}} \sum_j N_j \sum'_{l_x, l_y = -\infty}^{\infty} \frac{1}{r^{5/2}} \left[(2y_{ij0}^2 - x_{ij0}^2 - z_{ij0}^2) m_j^y + 3x_{ij0}y_{ij0} m_j^x + 3y_{ij0}z_{ij0} m_j^z \right], \quad (\text{A.19})$$

$$B_i^{z,\text{dip}} = \mu_{\text{at}} \sum_j N_j \sum'_{l_x, l_y = -\infty}^{\infty} \frac{1}{r^{5/2}} \left[(2z_{ij0}^2 - x_{ij0}^2 - y_{ij0}^2) m_j^z + 3x_{ij0}z_{ij0} m_j^x + 3y_{ij0}z_{ij0} m_j^y \right]. \quad (\text{A.20})$$

The unit vector $\mathbf{m}_j = \mathbf{M}_j/N_j = (m_j^x, m_j^y, m_j^z) = (\sin \theta_j \cos \phi_j, \sin \theta_j \sin \phi_j, \cos \theta_j)$ determines the direction of the particle magnetic moment, with θ_j and ϕ_j the polar and azimuthal angles.

Introducing now the lattice sums $T_{ij}^{\alpha\beta\gamma}$ and after some algebra one obtains for the three components of the dipole field

$$\begin{aligned} B_i^{x,\text{dip}} = & \mu_{\text{at}} \sum_j N_j \left\{ \left(2T_{ij}^{520} - T_{ij}^{502} - z_{ij0}^2 T_{ij}^{500} \right) m_j^x + 3T_{ij}^{511} m_j^y + 3z_{ij0} T_{ij}^{510} m_j^z \right. \\ & + \frac{5}{2} \left[\left(14T_{ij}^{940} - 10T_{ij}^{720} - 7T_{ij}^{922} + T_{ij}^{702} + z_{ij0}^2 (T_{ij}^{700} - 7T_{ij}^{920}) + \frac{4}{5} T_{ij}^{500} \right) m_j^x \right. \\ & + (21T_{ij}^{931} - 9T_{ij}^{711}) m_j^y + z_{ij0} (21T_{ij}^{930} - 9T_{ij}^{710}) m_j^z \left. \right] \left(\langle x_i^2 \rangle + \langle x_j^2 \rangle \right) \\ & + \frac{5}{2} \left[\left(14T_{ij}^{922} - 2T_{ij}^{720} - 7T_{ij}^{904} + 5T_{ij}^{702} + z_{ij0}^2 (T_{ij}^{700} - 7T_{ij}^{902}) - \frac{2}{5} T_{ij}^{500} \right) m_j^x \right. \\ & + (21T_{ij}^{913} - 9T_{ij}^{711}) m_j^y + z_{ij0} (21T_{ij}^{912} - 3T_{ij}^{710}) m_j^z \left. \right] \left(\langle y_i^2 \rangle + \langle y_j^2 \rangle \right) \end{aligned}$$

$$\begin{aligned}
& + \frac{5}{2} \left[\left(14 z_{ij0}^2 T_{ij}^{920} - 2 T_{ij}^{720} - 7 z_{ij0}^2 T_{ij}^{902} + T_{ij}^{702} + z_{ij0}^2 (5 T_{ij}^{700} - 7 z_{ij0}^2 T_{ij}^{900}) - \frac{2}{5} T_{ij}^{500} \right) m_j^x \right. \\
& \left. + (21 z_{ij0}^2 T_{ij}^{911} - 3 T_{ij}^{711}) m_j^y + z_{ij0} (21 z_{ij0}^2 T_{ij}^{910} - 9 T_{ij}^{710}) m_j^z \right] \left(\langle z_i^2 \rangle + \langle z_j^2 \rangle \right) \Big\}, \tag{A.21}
\end{aligned}$$

$$\begin{aligned}
B_i^{y,\text{dip}} &= \mu_{at} \sum_j N_j \left\{ 3 T_{ij}^{511} m_j^x + \left(2 T_{ij}^{502} - T_{ij}^{520} - z_{ij0}^2 T_{ij}^{500} \right) m_j^y + 3 z_{ij0} T_{ij}^{501} m_j^z \right. \\
& + \frac{5}{2} \left[\left(14 T_{ij}^{922} - 2 T_{ij}^{702} - 7 T_{ij}^{940} + 5 T_{ij}^{720} + z_{ij0}^2 (T_{ij}^{700} - 7 T_{ij}^{920}) - \frac{2}{5} T_{ij}^{500} \right) m_j^y \right. \\
& \left. + (21 T_{ij}^{931} - 9 T_{ij}^{711}) m_j^x + z_{ij0} (21 T_{ij}^{921} - 9 T_{ij}^{701}) m_j^z \right] \left(\langle x_i^2 \rangle + \langle x_j^2 \rangle \right) \\
& + \frac{5}{2} \left[\left(14 T_{ij}^{904} - 10 T_{ij}^{702} - 7 T_{ij}^{922} + T_{ij}^{720} + z_{ij0}^2 (T_{ij}^{700} - 7 T_{ij}^{902}) + \frac{4}{5} T_{ij}^{500} \right) m_j^y \right. \\
& \left. + (21 T_{ij}^{913} - 9 T_{ij}^{711}) m_j^x + z_{ij0} (21 T_{ij}^{903} - 9 T_{ij}^{701}) m_j^z \right] \left(\langle y_i^2 \rangle + \langle y_j^2 \rangle \right) \\
& + \frac{5}{2} \left[\left(14 z_{ij0}^2 T_{ij}^{902} - 2 T_{ij}^{702} - 7 z_{ij0}^2 T_{ij}^{920} + T_{ij}^{720} + z_{ij0}^2 (5 T_{ij}^{700} - 7 z_{ij0}^2 T_{ij}^{900}) - \frac{2}{5} T_{ij}^{500} \right) m_j^y \right. \\
& \left. + (21 z_{ij0}^2 T_{ij}^{911} - 3 T_{ij}^{711}) m_j^x + z_{ij0} (21 z_{ij0}^2 T_{ij}^{901} - 9 T_{ij}^{701}) m_j^z \right] \left(\langle z_i^2 \rangle + \langle z_j^2 \rangle \right) \Big\}, \tag{A.22}
\end{aligned}$$

$$\begin{aligned}
B_i^{z,\text{dip}} &= \mu_{at} \sum_j N_j \left\{ \left(2 z_{ij0}^2 T_{ij}^{500} - T_{ij}^{520} - T_{ij}^{502} \right) m_j^z + 3 z_{ij0} \left(T_{ij}^{510} m_j^x + T_{ij}^{501} m_j^y \right) \right. \\
& + \frac{5}{2} \left[\left(14 z_{ij0}^2 T_{ij}^{920} - 2 z_{ij0}^2 T_{ij}^{700} - 7 T_{ij}^{940} + 5 T_{ij}^{720} - 7 T_{ij}^{922} + T_{ij}^{702} - \frac{2}{5} T_{ij}^{500} \right) m_j^z \right. \\
& \left. + z_{ij0} (21 T_{ij}^{930} - 9 T_{ij}^{710}) m_j^x + z_{ij0} (21 T_{ij}^{921} - 3 T_{ij}^{701}) m_j^y \right] \left(\langle x_i^2 \rangle + \langle x_j^2 \rangle \right) \\
& + \frac{5}{2} \left[\left(14 z_{ij0}^2 T_{ij}^{902} - 2 z_{ij0}^2 T_{ij}^{700} - 7 T_{ij}^{904} + 5 T_{ij}^{702} - 7 T_{ij}^{922} + T_{ij}^{720} - \frac{2}{5} T_{ij}^{500} \right) m_j^z \right. \\
& \left. + z_{ij0} (21 T_{ij}^{912} - 3 T_{ij}^{710}) m_j^x + z_{ij0} (21 T_{ij}^{903} - 9 T_{ij}^{701}) m_j^y \right] \left(\langle y_i^2 \rangle + \langle y_j^2 \rangle \right) \\
& + \frac{5}{2} \left[\left(z_{ij0}^2 \left(14 z_{ij0}^2 T_{ij}^{900} - 10 T_{ij}^{700} - 7 T_{ij}^{920} - 7 T_{ij}^{902} \right) + T_{ij}^{720} + T_{ij}^{702} + \frac{4}{5} T_{ij}^{500} \right) m_j^z \right. \\
& \left. + z_{ij0} (21 z_{ij0}^2 T_{ij}^{910} - 9 T_{ij}^{710}) m_j^x + z_{ij0} (21 z_{ij0}^2 T_{ij}^{901} - 9 T_{ij}^{701}) m_j^y \right] \left(\langle z_i^2 \rangle + \langle z_j^2 \rangle \right) \Big\}. \tag{A.23}
\end{aligned}$$

The lateral extensions L_x and L_y of the unit cell and the components x_{ij0} and y_{ij0} of the interparticle distances within a unit cell are involved in a complicated manner in the lattice sums $T_{ij}^{\alpha\beta\gamma}$, whereas the dependence on the vertical distances z_{ij0} appears explicitly. Note that the contributions from mirror particles $i = j$ located in different unit cells are taken into account. The expressions for the dipole field components, equations A.21 – A.23, are simplified appreciably if all particles are located in the same plane ($z_{ij0} = 0$). In this case $B_i^{z,\text{dip}} \propto m_j^z$, hence the z component of the dipole field vanishes for an in-plane magnetization ($m_j^z = 0$). As before, the point-dipole sum is recovered by setting $\langle x_i^2 \rangle = 0$, etc. The dipole energy E_{dip} per unit cell is obtained from equation 1 by performing the sum over all particles $i = 1 \dots n$ in the unit cell.

References

- [1] For a review see: Dormann J L, Fiorani D and Tronc E 1997 *Adv. Chem. Phys.* **98** 283
- [2] Sun S, Murray C B, Weller D, Folks L and Moser A 2000 *Science* **287** 1989; Respaud M et al. 1998 *Phys. Rev. B* **57** 2925; Giersig M and Hilgersdorff M 1999 *J. Phys. D* **32** L111; Russier V, Petit C, Legrand J and Pileni M P 2000 *Phys. Rev. B* **62** 3910
- [3] Weili Luo, Nagel S R, Rosenbaum T F and Rosensweig R E 1991 *Phys. Rev. Lett.* **67** 2721; Djurberg C, Svedlindh P, Nordblad P, Hansen M F, Bødker F and Mørup S 1997 *Phys. Rev. Lett.* **79** 5154; Martinez B, Obradors X, Balcells L, Rouanet A and Monty C 1997 *Phys. Rev. Lett.* **80** 181; Mamiya H, Nakatani I and Furubayashi T 1999 *Phys. Rev. Lett.* **82** 4332; Garcia del Muro M, Battle X and Labarta A 1999 *Phys. Rev. B* **59** 13 584; Jönsson P, Hansen M F and Nordblad P 2000 *Phys. Rev. B* **61** 1261
- [4] Jinlong Zhang, Boyd C and Weili Luo 1996 *Phys. Rev. Lett.* **77** 390
- [5] Andersson J O, Djurberg C, Jonsson T, Svedlindh P and Nordblad P 1997 *Phys. Rev. B* **56** 13 983; Chantrell R W, Walmsley N, Gore J and Maylin M 2000 *Phys. Rev. B* **63** 024410; Kechrakos D and Trohidou K N *Phys. Rev. B* **58** 12 169
- [6] Hansen M F and Mørup S 1998 *J. Magn. Magn. Mater.* **184** 262
- [7] Dormann J L, Fiorani D and Tronc E 1999 *J. Magn. Magn. Mater.* **202** 251
- [8] Lomba E, Lado F and Weis J J 2000 *Phys. Rev. E* **61** 3838
- [9] Belobrov P, Gekht R S and Ignatchenko V A 1983 *Sov. Phys. JETP* **57** 636
- [10] Prakash S and Henley C L 1990 *Phys. Rev. B* **42** 6574
- [11] Rozenbaum V M, Ogenko V M and Chuiko A A 1991 *Sov. Phys. Usp.* **34** 883
- [12] Politi P and Pini M G 2002 *Phys. Rev. B* **66** 214414
- [13] Villain J, Bidaux R, Carton J P and Conte R, *J. Phys. (Paris)* **41**, 1263 (1980); Henley C L 1989 *Phys. Rev. Lett.* **62** 2056
- [14] De'Bell K, MacIsaac A B, Booth I N and Whitehead J P 1997 *Phys. Rev. B* **55** 15 108; Abu-Labdeh A M, Whitehead J P, De'Bell K and MacIsaac A B 2001 *Phys. Rev. B* **65** 024434; Carbognani A, Rastelli E, Regina S and Tassi A 2000 *Phys. Rev. B* **62** 1015
- [15] Mermin N M and Wagner H 1966 *Phys. Rev. Lett.* **17** 1133
- [16] Yafet Y, Kwo J and Gyorgy E M (1986) *Phys. Rev. B* **33** 6519
- [17] Binder K and Young A P 1986 *Rev. Mod. Phys.* **58** 801
- [18] Bovensiepen U, Pouloupoulos P, Platow W, Farle M and Baberschke K 1999 *J. Magn. Magn. Mater.* **192** L386
- [19] Stoner E C and Wohlfarth E P 1948 *Trans. Roy. Soc. A* **240** 599
- [20] Jensen P J 1997 *Ann. Physik* **6** 317
- [21] *Numerical Recipes*, Cambridge University Press 1992
- [22] Chantrell R W, Coverdale G N, El Hilo M and O'Grady K 1996 *J. Magn. Magn. Mater.* **157/158** 250; Weis J J and Levesque D 1993 *Phys. Rev. Lett.* **71** 2729
- [23] Schwarzacher W, private communication
- [24] Jensen P J and Pastor G M 2002 *Phys. Stat. Sol. (a)* **189** 527
- [25] Jensen P J, unpublished
- [26] Pogorelov Y G, private communication